A Complete Tool for Analyzing Mutual Couplings in Nonuniform Arrays of Rectangular Aperture Radiators

Wang, Zhengzheng; Simeoni, Massimiliano; Lager, Ioan E.

DOI
10.1109/LAWP.2017.2768225

Publication date
2017

Document Version
Accepted author manuscript

Published in
IEEE Antennas and Wireless Propagation Letters

A Complete Tool for Analyzing Mutual Couplings in Nonuniform Arrays of Rectangular Aperture Radiators

Zhengzheng Wang, Massimiliano Simeoni, *Member, IEEE*, and Ioan E. Lager, *Senior Member, IEEE*

***Abstract*—A complete tool for analyzing the mutual coupling in nonuniform (interleaved) array antennas consisting of rectangular aperture radiators is discussed. It relies on deriving the coupling admittances between arbitrarily located apertures via a two-dimensional interpolation scheme. Realistic radiators are accounted for through their scattering matrix evaluated by means of full-wave analyses. The method yields accurate results while greatly reducing the computation time. Its validity is demonstrated against measurements done on a medium-sized, interleaved, nonuniform array of cavity-backed apertures.**

***Index Terms*—Antenna arrays, aperture antennas, mutual coupling.**

I. Introduction

NONUNIFORM array antennas receive increasing attention due to their range of performance enhancements, with shared apertures being particularly attractive for implementing multifunctionality via subarray interleaving. Obtaining such operational benefits requires intricate design methodologies. Undoubtedly, there are many placement strategies yielding arrays complying to extremely challenging specifications. However, the majority of these schemes employ ideal, isotropic radiators, and their effectiveness drops rapidly when mutual coupling or the behavior of realistic radiators are accounted for. The design of large, nonuniform, realistic arrays remains a hard problem, with [1] and [2] discussing some of the few available solutions.

This letter proposes an effective answer to this challenge. It builds upon the generalized admittance matrix (GAM)-based mutual coupling evaluation discussed in [3] and [4, Sec. 7.3.3] and an interpolation technique inspired by [5] (that applied it for reducing the complexity of array measurements), and also used in [1] for drastically lowering run-times. The potential of combining these elements was demonstrated in [6]. This avenue is now used for developing a complete tool for evaluating the mutual coupling in nonuniform array antennas. Its main novelty elements are: 1) providing clear, effective rules for selecting the locations of the testing apertures employed for constructing the interpolation scheme, and 2) embedding the behavior of realistic radiators in the array's scattering representation. The tool's performance will be validated by comparing its results with measurement data concerning a shared aperture antenna consisting of two interleaved, nonuniform subarrays.

Manuscript received September 25, 2017; revised October 23, 2017; accepted October 24, 2017. Date of publication November 2, 2017; date of current version December 11, 2017. *(Corresponding author: Ioan E. Lager.)*

Z. Wang and I. E. Lager are with the Faculty of Electrical Engineering, Mathematics and Computer Science, Delft University of Technology, Delft 2628 CD, The Netherlands (e-mail: z.wang-11@student.tudelft.nl; i.e.lager@tudelft.nl).

M. Simeoni is with the European Space Agency, European Space Research and Technology Centre, Noordwijk 2200 AG, The Netherlands (e-mail: massimiliano.simeoni@esa.int).

II. Analysis Strategy

The examined array antenna[1] consists of N_e waveguide-end, rectangular apertures in an infinitely extended, perfectly conducting flange. The flange is at $z = 0$, the array radiating towards $z > 0$. The apertures are of dimensions $a_i \times b_i$ ($a_i \geqslant b_i$), $i = 1, \ldots, N_\mathrm{e}$, with reference centers at $\boldsymbol{r}_i = x_i\hat{\boldsymbol{x}} + y_i\hat{\boldsymbol{y}}$ and normals $\hat{\boldsymbol{n}}_i = \hat{\boldsymbol{z}}$. The waveguides' longitudinal axes are also along $\hat{\boldsymbol{z}}$. Excitation is time-harmonic, with frequency f and angular frequency $\omega = 2\pi f$. Materials are characterized by the permittivity $\varepsilon = \varepsilon_\mathrm{r}\varepsilon_0$ and the permeability $\mu = \mu_\mathrm{r}\mu_0$. The following quantities apply to free space: wavespeed $c_0 = (\varepsilon_0\mu_0)^{-1/2}$, wavenumber $k_0 = \omega/c_0$, wavelength $\lambda_0 = c_0/f$, and wave impedance $Y_0 = (\mu_0/\varepsilon_0)^{-1/2}$.

The array may consist of N_sa subarrays of identical and aligned radiators. In all practical cases N_sa is small ($N_\mathrm{sa} = 2$ for the study in Section III). For clarity, this analysis is confined to subarrays with either horizontal "H" or vertical "V" elements, having a_i edges along either $\hat{\boldsymbol{x}}$ or $\hat{\boldsymbol{y}}$, only.

The electromagnetic (EM) examination of this type of array antenna is known to be a hard problem: 1) resorting to an analytic representation via Floquet modes [7] is ruled out by the configuration's irregularity; and 2) a full-wave study via standard EM software becomes quickly computationally prohibitive even for medium-sized arrays.

To sidestep these roadblocks, the EM field at the waveguide-ends is expanded in terms of rectangular waveguide modes as defined in [8, Ch. 1]. The modal coupling admittances can be calculated analytically, but the procedure is computationally extremely expensive. Nevertheless, waveguide-end radiators can be construed as minimally scattering according to the interpretation in [9]. The coupling admittances between any *identical* pair of modes can then be expressed via a two-dimensional interpolation based on only nine *reference couplings* that are evaluated analytically. For small N_sa's, this strategy allows assembling expeditiously the $\mathrm{GAM}_\mathrm{rad}$ of the complete radiating

[1]Position in the configuration is specified by the coordinates $\{x, y, z\}$ with respect to a background Cartesian reference frame with origin O and three mutually orthogonal unit vectors $\{\hat{\boldsymbol{x}}, \hat{\boldsymbol{y}}, \hat{\boldsymbol{z}}\}$ that, in this order, form a right-handed system. The position vector is $\boldsymbol{r} = x\hat{\boldsymbol{x}} + y\hat{\boldsymbol{y}} + z\hat{\boldsymbol{z}}$, with $|\boldsymbol{r}| = r$.

aperture even for very large, nonuniform arrays, with $\mathrm{GAM}_{\mathrm{rad}}$ yielding, in turn, the array's scattering matrix. These steps will be henceforth elaborated upon.

A. Coupling Admittance Between Rectangular Apertures

For convenience, the double-index notation of rectangular waveguide modes is coalesced into a single-index notation m ($m \leqslant M$), with the modes being ordered in increasing cutoff frequency $f_{\mathrm{c};m}$ sequence. With this notation, following [3], the coupling admittance $Y(m, i, n, j)$ between the mode m on the aperture $\mathcal{A}_i$ and the mode n on the aperture $\mathcal{A}_j$ reads

$$Y(m,i,n,j) = \frac{\mathrm{j}k_0 Y_0}{[Y(m,i)Y(n,j)]^{-1/2}} \times \iint_{\mathcal{A}_i} \mathrm{d}x\mathrm{d}y \iint_{\mathcal{A}_j} [\boldsymbol{\Psi}(m,i)\cdot\boldsymbol{\Psi}(n,j)]\, G(|\boldsymbol{r}-\boldsymbol{r}'|)\,\mathrm{d}x'\mathrm{d}y' \tag{1}$$

in which $Y(p,q)$ is the longitudinal (wave) admittance of the mode p in the waveguide q, with $Y(p,q) = Y_0\,\gamma(p,q)/k_0$ for TE-modes and $Y(p,q) = Y_0\,\varepsilon_{\mathrm{r}}(q)\,k_0/\gamma(p,q)$ for TM-modes

$$\boldsymbol{\Psi}(p,q) = \boldsymbol{h}(p,q) + \hat{\boldsymbol{z}}\gamma(p,q)h_z(p,q)/k_0 \tag{2}$$

with $\boldsymbol{h}(p,q)$ and $h_z(p,q)$ being the transverse and longitudinal modal vector components [8], respectively, and

$$G(|\boldsymbol{r}-\boldsymbol{r}'|) = \exp\left(-\mathrm{j}k_0|\boldsymbol{r}-\boldsymbol{r}'|\right)/4\pi|\boldsymbol{r}-\boldsymbol{r}'| \tag{3}$$

is the free-space Green's function, with $\boldsymbol{r}\in\mathcal{A}_i$ and $\boldsymbol{r}'\in\mathcal{A}_j$.

$$\gamma(p,q) = \left[k_0^2\varepsilon_{\mathrm{r}}(q) - k_{\mathrm{c}}^2(p,q)\right]^{-1/2} \tag{4}$$

is the propagation constant of the mode p in the waveguide q, with $k_{\mathrm{c}}^2(p,q)$ being the corresponding cutoff wavenumber [8]. The expression in (1) can be transformed as (see [3])

$$Y(m,i,n,j) = 2\pi^2\mathrm{j}\,k_0 Y_0\,A_{m,n}A_{m',n'}\sum_{\alpha=x,y,z} c_\alpha I_\alpha \tag{5}$$

in which $A_{p,q}$ are given in [8, Table 1.2], c_α are given in [3, Table 1], and

$$\begin{bmatrix} I_x \\ I_y \\ I_z \end{bmatrix} = \iint_{\mathcal{A}_i}\mathrm{d}x\mathrm{d}y\iint_{\mathcal{A}_j}\mathrm{d}x'\mathrm{d}y'\,G(|\boldsymbol{r}-\boldsymbol{r}'|) \times \begin{bmatrix} \sin \\ \cos \\ \cos \end{bmatrix}\left(\frac{m\pi x}{a_i}\right)\begin{bmatrix} \cos \\ \sin \\ \cos \end{bmatrix}\left(\frac{n\pi y}{b_i}\right)\begin{bmatrix} \sin \\ \cos \\ \cos \end{bmatrix}\left(\frac{m'\pi x'}{a_j}\right)\begin{bmatrix} \cos \\ \sin \\ \cos \end{bmatrix}\left(\frac{n'\pi y'}{b_j}\right). \tag{6}$$

As in [3], the quadruple integral in (6) is reduced to a double integral by using the change of variables in [10, Sec. 6.1] and analytically effectuating two of the ensuing integrals. The resulting expression was implemented in a MATLAB code.

B. Interpolation Approach to the Analysis of Arrays Consisting of Rectangular Apertures

The direct evaluation of couplings via (6) becomes quickly computationally prohibitive as the number of coupled apertures increases. This situation is effectively precluded via an interpolation strategy inspired by [5]. In line with [6], a reference aperture $\mathcal{A}_{i_0}$, centered at $\boldsymbol{r}_{i_0} = x_0\hat{\boldsymbol{x}} + y_0\hat{\boldsymbol{y}}$, is first selected. Let then another aperture $\mathcal{A}_j$ centered at a location $\boldsymbol{r}_j$ complying to the condition $\varphi = \arccos(\boldsymbol{r}'\cdot\hat{\boldsymbol{x}}/r') \in [0, \pi/2]$, with $\boldsymbol{r}' = \boldsymbol{r}_j - \boldsymbol{r}_{i_0}$ and $r' = |\boldsymbol{r}'|$. The coupling admittance between the mode m on $\mathcal{A}_{i_0}$ and the mode n on $\mathcal{A}_j$ is generically expressed as

$$\begin{aligned}\tilde{Y}(m,i_0,n,j) = {} & \exp(-\mathrm{j}k_0 r') \\ & \times\left[\left(A_1/\xi + A_2/\xi^2 + A_3/\xi^3\right)\cos^2(\varphi)\right. \\ & + \left(A_4/\xi + A_5/\xi^2 + A_6/\xi^3\right)\sin^2(\varphi) \\ & \left. + \left(A_7/\xi + A_8/\xi^2 + A_9/\xi^3\right)\sin^2(2\varphi)\right]\end{aligned} \tag{7}$$

where $A_1, \ldots, A_9$ are interpolation coefficients and $\xi = k_0 r'$. Clearly, the applicability of (7) can be extended to any aperture $\mathcal{A}_j$ by making use of the relation's even symmetry with respect to the planes $x = x_0$ and $y = y_0$.

The interpolation coefficients are inferred from the $m \to n$ coupling admittances between $\mathcal{A}_{i_0}$ and nine testing apertures $\mathcal{A}_{\mathrm{t};1}, \ldots, \mathcal{A}_{\mathrm{t};9}$ that are congruent with $\mathcal{A}_j$ and centered:

1) $\mathcal{A}_{\mathrm{t};1\div3}$: at $(x_0 + d_{x;1}, y_0)$, $(x_0 + d_{x;2}, y_0)$ and $(x_0 + d_{x;3}, y_0)$, with $0 < d_{x;1} < d_{x;2} < d_{x;3}$;
2) $\mathcal{A}_{\mathrm{t};4\div6}$: at $(x_0, y_0 + d_{y;1})$, $(x_0, y_0 + d_{y;2})$ and $(x_0, y_0 + d_{y;3})$, with $0 < d_{y;1} < d_{y;2} < d_{y;3}$;
3) $\mathcal{A}_{\mathrm{t};7\div9}$: along the bisector of $y = y_0$ and $x = x_0$, at distances $0 < d_{\mathrm{i};1} < d_{\mathrm{i};2} < d_{\mathrm{i};3}$ from $\boldsymbol{r}_{i_0}$ and with $x_0 < x_{\mathrm{i};1} < x_{\mathrm{i};2} < x_{\mathrm{i};3}$ ("right" of $\boldsymbol{r}_{i_0}$).

The nine reference couplings calculated via (6) for $\mathcal{A}_{\mathrm{t};1}, \ldots, \mathcal{A}_{\mathrm{t};9}$ are filled in (7), and $A_1, \ldots, A_9$ then follow by solving the resulting system of nine linear equations. The overhead of calculating the reference couplings is quickly recovered for large arrays, the evaluation of (7) requiring insignificant time. Moreover, $A_1, \ldots, A_9$ can be stored and reused for studying any array comprising the relevant combination of apertures.

Experience shows that the interpolation scheme's accuracy is largely influenced by the choice for the locations of the testing apertures. The following heuristic rules for selecting the reference centers of $\mathcal{A}_{\mathrm{t};1}, \ldots, \mathcal{A}_{\mathrm{t};9}$ were arrived at based on simulations carried out on a wide range of element placements:

1) "H"↔"H" couplings (also applicable to "V"↔"V" couplings, by applying a $\pi/2$ rotation)
   $d_{x;1} = \delta_1 = (a_{i_0} + a_j)/2$, $d_{x;2} = 0.84\lambda_0$, $d_{x;3} = 3\lambda_0$;
   $d_{y;1} = \delta_2 = (b_{i_0} + b_j)/2$, $d_{y;2} = 0.84\lambda_0$, $d_{y;3} = 3\lambda_0$;
   $d_{\mathrm{i};1} = \sqrt{2}\min(\delta_1, \delta_2)$, $d_{\mathrm{i};2} = \lambda_0$, $d_{\mathrm{i};3} = 3\lambda_0$.
2) "H"↔"V" couplings
   $d_{x;1} = \delta = (a_{i_0} + b_j)/2$, $d_{x;2} = \lambda_0$, $d_{x;3} = 2.8\lambda_0$;
   $d_{y;1} = \delta$, $d_{y;2} = \lambda_0$, $d_{y;3} = 2.8\lambda_0$;
   $d_{\mathrm{i};1} = \sqrt{2}\left[\min(a_{i_0}, b_j)/2 + \delta\right]$, $d_{\mathrm{i};2} = \lambda_0$, $d_{\mathrm{i};3} = 3\lambda_0$.

The interpolation accuracy was assessed based on the deviation $\Delta_Y = ||Y(m,i,n,j)| - |\tilde{Y}(m,i,n,j)||/\max(|Y(m,i,n,j)|)$, with $Y(m,i,n,j)$ being calculated via (6) and $\tilde{Y}(m,i,n,j)$ via (7). For nonoverlapping apertures of the type examined in Section III, $\Delta_Y < 1.5\%$ for "H–H" couplings and $\Delta_Y < 20\%$ for "H–V" couplings. The larger "H–V" Δ_Y's are due to several "H–V" $Y(m,i,n,j)$'s being zero in both $\hat{\boldsymbol{x}}$- and $\hat{\boldsymbol{y}}$-directions, leaving only the diagonal couplings as a basis for interpolation–this does not apply to "H–H" combinations. However, Δ_Y decreases rapidly with increasing spacing, and the deviation was below 0.2% for the entire array in Fig. 1.

C. Assembling of the Array's Scattering Matrices

$\mathrm{GAM}_{\mathrm{rad}}$ directly yields the radiation scattering matrix S_{rad} that, by using the analytic expressions of the EM field radiated by rectangular waveguide modes [11, Sec. 18.1], allows assessing the array's radiation and scanning performance. Next, the

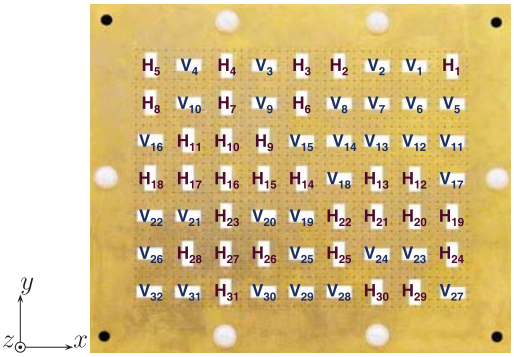

Fig. 1. Polarization-agile antenna—front view, with the element counting, per subarray. The lattice is uniform in the $\hat{\boldsymbol{x}}$- and $\hat{\boldsymbol{y}}$-directions, with identical lattice steps $\Delta = 15\,\text{mm}$.

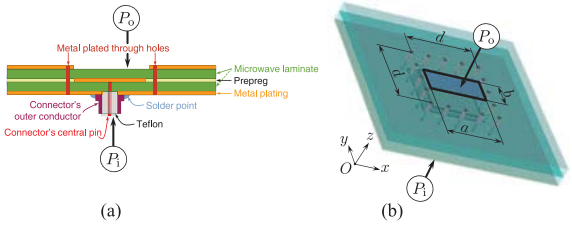

Fig. 2. Polarization-agile antenna element. (a) Cross section showing the internal stratification; (b) scale illustration of the radiator. Main dimensions: $a = 9.7\,\text{mm}$, $b = 4.3\,\text{mm}$ $d = 11.7\,\text{mm}$; the through-vias are spaced at $v_\text{s} = 2.925\,\text{mm}$; the embedded patch has the dimensions $p_x = 8.4\,\text{mm}$ and $p_y = 8.4\,\text{mm}$, is symmetrically placed with respect to the $x = 0$ plane, and it is off-center by $s_y = 1.6\,\text{mm}$. P_i and P_o denote the feeding coaxial port (input) and the rectangular aperture, radiating port (output), respectively.

elementary radiators are accounted for, with [4, Sec. 7.3.3] or [12] providing guidelines to this end. However, a more realistic avenue is employing the scattering matrices S_el of genuine radiators derived via back-to-back, full-wave simulations. The combination of S_rad and S_el yields the complete array's scattering matrix S_arr and, thus, the active reflection coefficients at the feeding ports. These combined facilities render this strategy instrumental for embedding full EM characterization within array optimization schemes.

III. Practical Application

The strategy discussed in Section II is now applied to the study of an array antenna consisting of radiating rectangular apertures. The effectiveness of the computational approach is assessed by comparing simulated and measured results.

A. Polarization-Agile Array Antenna

The investigated device is a shared aperture array implementing the polarization agility principle introduced in [13, Sec. 6]. The array is partitioned into two interleaved subarrays of 32 and 31 *identical elements*, respectively (see Fig. 1). The elements in the subarrays are rotated by 90° with respect to each other for generating the vertical ("V") and horizontal ("H") EM field components. This study is confined to the antenna front end, each element being individually accessible via SMA connectors. The radiators are cavity-backed aperture antennas excited by embedded pin-fed patches (see Fig. 2). The array is fabricated in printed circuit board (PCB) technology by using a

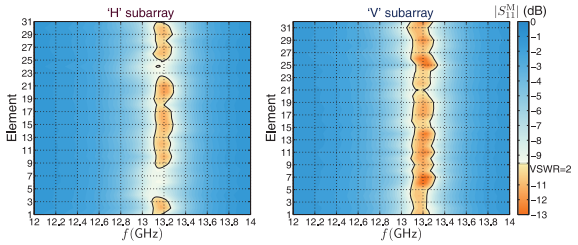

Fig. 3. Measured reflection coefficients for the subarrays in Fig. 1.

multilayer sandwich of RO4350B laminates [14]. All through-vias are metal-plated through holes. The SMA connectors are soldered with a pick-and-place machine.

The reflection coefficients at all 63 feeding ports were measured via a setup comprising an Agilent Technologies E8364B vector network analyzer and an Agilent Technologies 87050-K24 full 2×24 crossbar mechanical switch test-set. The switch test-set was connected to the elementary radiators via 2 m calibrated cables, with the remaining ports being closed on matched loads. The array was placed inside an enclosure with absorber-padded inner walls for minimizing environmental impact. The measurement results are reported in Fig. 3. The variations in the elements' embedding are clearly visible—they translate in both variable matching levels and in slight variations of the pertaining resonant frequencies. The best matching is observed for the elements H_{21} and H_{27} (H-subarray) and V_7, V_{14}, and V_{29} (V-subarray). Note that these elements have an almost uniform immediate neighborhood. Another interesting feature concerns the linear array H_4, H_7, H_{10}, H_{16}, H_{23}, H_{27}, and H_{31}, the only full column pertaining to the same subarray. In it, matching runs from $|S_{11}^\text{M}| \approx -9\,\text{dB}$ for H_7[2] up to $|S_{11}^\text{M}| \approx -11\,\text{dB}$ for H_{27}, with no regularity. The resonant frequencies vary between 13.11 and 13.25 GHz, with a mean of $f_\text{r;m} = 13.19\,\text{GHz}$ and a standard deviation $\sigma = 28.4\,\text{MHz}$. This behavior is illustrative for the challenges entailed by the design of such highly irregular arrays.

B. Numerical Implementation

The computational strategies in Sections II-A and II-B were implemented in MATLAB. The couplings between the TEM mode at P_i and the aperture modes at P_o (see Fig. 2) were evaluated via a back-to-back, time-harmonic CST Microwave Studio (CST) simulation. Assembling GAM_rad via interpolation, calculating S_rad and aggregating S_arr were all coded in MATLAB. The feature computation times on a workstation with a 3.1 GHz processor and 32 GB internal memory are given in Table I. The most remarkable observation is the *2200-fold* run-time reduction when assembling GAM_rad via interpolation, when compared to the direct analytical evaluation. As for purely computational approaches, comparisons are immaterial since coding the investigated configuration in commonly used EM analysis packages exceeds the memory capabilities of even large workstations. Note that the overhead steps 1 and 2 are needed only once for any given aperture antenna type, that data being amenable to being saved and reused. Only the computationally extremely effective steps 3, 4, and (possibly) 5 need being repeated in optimization iterative schemes.

[2]The reflection coefficient at any coaxial feeding port is generically referred to as S_{11}, supplemented by the port's identifier. The descriptive superscripts "M" and "S" denote "measured" and "simulated," respectively.

TABLE I
FEATURE COMPUTATION TIMES FOR 100 FREQUENCY SAMPLES

	Algorithm's block	Computation time
1	Reference aperture modal coupling evaluation **4 coupling types × 9 apertures × 10 modes**	29 ½ min
2	Calculation of S_{el} via CST simulation	12 ½ min
3	Assembling GAM_{rad} via interpolation **63 apertures × 10 modes**	5.7 s
4	Converting GAM_{rad} into S_{rad}	19.1 s
5	Combining S_{rad} and S_{el} into S_{arr}	110 s
	Assembling GAM_{rad} by analytical evaluation **63 apertures × 10 modes**	**35½ h**

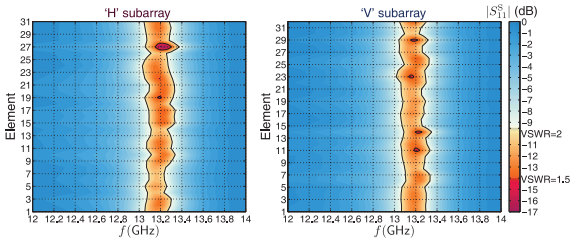

Fig. 4. Simulated reflection coefficients for the subarrays in Fig. 1.

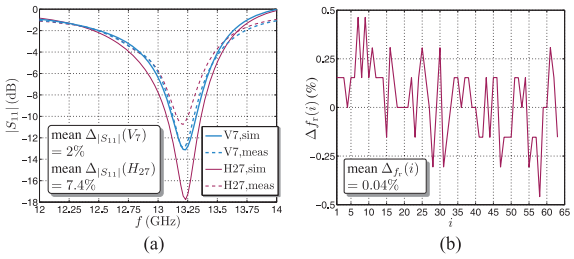

(a) (b)

Fig. 5. Deviations between measured and simulated results. (a) Comparison of $|S^{\text{M}}_{11}|$ and $|S^{\text{S}}_{11}|$ for the elements with the best (V_7) and worst (H_{27}) approximations; (b) resonant frequency deviations. $\Delta_{|S_{11}|}(i) = |S^{\text{M}}_{11,\text{dB}}(i) - S^{\text{S}}_{11,\text{dB}}(i)| / \max_{\forall i'}(|S^{\text{S}}_{11,\text{dB}}(i')|)$, mean calculated over the frequency band.

C. Validation of the Numerical Analysis

The accuracy of the proposed computational approach was validated by comparing the simulated reflection coefficients at the individual input ports with the measured results in Fig. 3. The simulated results are shown in Fig. 4. Note that a relative permittivity tuning was needed for fitting the simulated results, the computational relative permittivity of the material being known to slightly deviate from the measured one [14].

The overall features of the plots in Figs. 3 and 4, namely the matching level patterns and resonant frequency fluctuations, concur. However, the simulated resonance $|S_{11}|$ levels are about 3–4 dB below the measured ones. To better illustrate this, the smallest and largest differences are shown in Fig. 5(a). This discrepancy is attributed to: 1) the additional reflections caused by the actual SMA connectors and mounting imperfections that were not included in the CST model; 2) the simulations assume an infinitely extended flange and cannot account for reflections caused by the edges of a finite flange; and 3) the measurement results were also affected by small, but nonnegligible reflections from the enclosure's walls.

As a quantitative measure of the good agreement between the simulated and measured results, the relative deviation $\Delta_{f_{\text{r}}}$ between the simulated $f^{\text{S}}_{\text{r}}(i)$ and measured $f^{\text{M}}_{\text{r}}(i)$ resonant frequencies pertaining to the input ports $i = 1, \ldots, N_{\text{e}}$ is plotted in Fig. 5(b). The maximum deviation is less than 0.5%, which is a convincing proof of the simulation's accuracy.

IV. CONCLUSION

A complete tool for evaluating the mutual coupling in nonuniform (interleaved) array antennas of rectangular aperture radiators was presented. The proposed two-dimensional interpolation scheme was shown to yield (well) under 10% deviations between interpolated and exact coupling admittances for technologically realistic arrays. Practical radiators were accounted for via their scattering matrix calculated with full-wave EM analysis tools. A 2200-fold computation time reduction with respect to a direct admittance calculation was observed. Comparisons with measurements effectuated on a medium-sized, interleaved, nonuniform array of cavity-backed apertures evidenced lower than 0.5% deviations between the simulated and measured resonant frequencies at the feeding ports. The advocated approach allows embedding full EM characterization within array optimization schemes.

REFERENCES

[1] D. González-Ovejero and C. Craeye, "Interpolatory macro basis functions analysis of non-periodic arrays," *IEEE Trans. Antennas Propag.*, vol. 59, no. 8, pp. 3117–3122, Aug. 2011.

[2] D. J. Ludick, R. Maaskant, D. B. Davidson, U. Jakobus, R. Mittra, and D. de Villiers, "Efficient analysis of large aperiodic antenna arrays using the domain Green's function method," *IEEE Trans. Antennas Propag.*, vol. 62, no. 4, pp. 1579–1588, Apr. 2014.

[3] T. S. Bird, "Analysis of mutual coupling in finite arrays of different-sized rectangular waveguides," *IEEE Trans. Antennas Propag.*, vol. 38, no. 2, pp. 166–172, Feb. 1990.

[4] T. S. Bird, *Fundamentals of Aperture Antennas and Arrays*, Chichester, U.K.: Wiley, 2016.

[5] M. C. Bailey, "Technique for extension of small antenna array mutual-coupling data to larger antenna arrays," NASA, Langley Res. Center, Hampton, VA, USA, NASA Tech. Paper 3606, Aug. 1996.

[6] I. E. Lager, M. Simeoni, and C. I. Coman, "Mutual coupling in non-uniform array antennas – An effective recipe," in *Proc. 6th EuCAP*, 2012, pp. 1518–1522.

[7] B. A. Munk, *Finite Antenna Arrays and FSS*, Hoboken, NJ, USA: Wiley, 2003.

[8] G. Conciauro, M. Gugliemi, and R. Sorrentino, *Advanced Modal Analysis. CAD Techniques for Waveguide Components and Filters*, Chichester, U.K.: Wiley, 2000.

[9] J. W. Wallace and R. Mehmood, "On the accuracy of equivalent circuit models for multi-antenna systems," *IEEE Trans. Antennas Propag.*, vol. 60, no. 2, pp. 540–547, Feb. 2012.

[10] L. Lewine, *Advanced Theory of Waveguides*, London, U.K.: Iliffe, 1951.

[11] S. J. Orfanidis, *Electromagnetic Waves and Antennas*, 2016. [Online]. Available: www.ece.rutgers.edu/∼orfanidi/ewa

[12] J. Rubio, M. A. González, and J. Zapata, "Generalized-scattering-matrix analysis of a class of finite arrays of coupled antennas by using 3-D FEM and spherical mode expansion," *IEEE Trans. Antennas Propag.*, vol. 53, no. 3, pp. 1133–1144, Mar. 2005.

[13] M. Simeoni, I. E. Lager, C. I. Coman, and A. G. Roederer, "Implementation of polarization agility in planar phased-array antennas by means of interleaved subarrays," *Radio Sci.*, vol. 44, RS5013, Oct. 2009. [Online]. Available: doi: 10.1029/2009RS004175.

[14] Rogers Corporation, "RO4350B laminates," [Online]. Available: http://www.rogerscorp.com/acs/products/55/RO4350B-Laminates.aspx